Journal of Hazardous Materials 388 (2020) 121788

Contents lists available at ScienceDirect

Journal of Hazardous Materials

journal homepage: www.elsevier.com/locate/jhazmat

Nanoplastics: From tissue accumulation to cell translocation into *Mytilus galloprovincialis* hemocytes. resilience of immune cells exposed to nanoplastics and nanoplastics plus *Vibrio splendidus* combination

M. Sendra[a], A. Saco[a], M.P. Yeste[b], A. Romero[a], B. Novoa[a], A. Figueras[a,*]

[a] Institute of Marine Research (IIM), National Research Council (CSIC), Eduardo Cabello 6, 36208, Vigo, Spain
[b] Department of Material Science, Metallurgical Engineering and Inorganic Chemistry, University of Cádiz, Spain

GRAPHICAL ABSTRACT

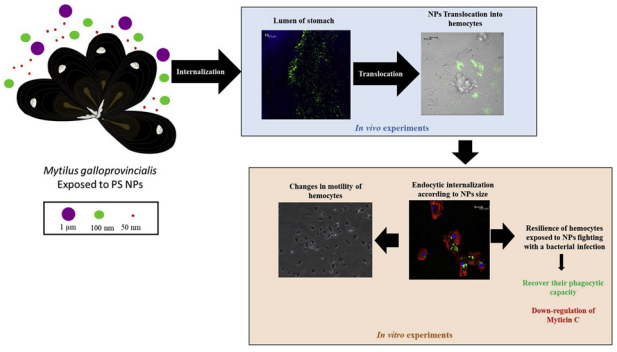

ARTICLE INFO

Editor: R Teresa

Keywords:
Mussel
Bioaccumulation
Endocytosis routes
Cell motility
V. splendidus

ABSTRACT

Plastic litter is an issue of global concern. In this work *Mytilus galloprovincialis* was used to study the distribution and effects of polystyrene nanoplastics (PS NPs) of different sizes (50 nm, 100 nm and 1 µm) on immune cells. Internalization and translocation of NPs to hemolymph were carried out by in vivo experiments, while endocytic routes and effects of PS NPs on hemocytes were studied in vitro. The smallest PS NPs tested were detected in the digestive gland and muscle. A fast and size-dependent translocation of PS NPs to the hemolymph was recorded after 3 h of exposure. The internalization rate of 50 nm PS NPs was lower when caveolae and clathrin endocytosis pathways were inhibited. On the other hand, the internalization of larger particles decreased when phagocytosis was inhibited. The hemocytes exposed to NPs had changes in motility, apoptosis, ROS and phagocytic capacity. However, they showed resilience when were infected with bacteria after PS NP exposure being able to recover their phagocytic capacity although the expression of the antimicrobial peptide Myticin C was reduced. Our findings show for the first time the translocation of PS NPs into hemocytes and how their effects trigger the loss of its functional parameters.

* Corresponding author.
E-mail addresses: antoniofigueras@iim.csic.es, antoniofigueras@csic.es (A. Figueras).

https://doi.org/10.1016/j.jhazmat.2019.121788
Received 8 October 2019; Received in revised form 27 November 2019; Accepted 28 November 2019
Available online 30 November 2019

1. Introduction

Nowadays, a world without plastic is inconceivable. Almost 348 million tonnes of plastic were produced in 2018 (PlasticsEurope, 2018). In addition, the production of plastic fibres is about 65 million tonnes per year (Salvador Cesa et al., 2017). The European production of Polystyrene (PS) was almost 2 million tonnes in 2018 (PlasticsEurope, 2018). In two of the most relevant plastic surveys, PS was found to be the most abundant plastic (Browne, 2008). Land sources such as mishandled plastic, waste water treatment plants, lakes, rivers and agriculture contribute between 70–80 % of the plastics found in the oceans (Alimi et al., 2018).

Fragmentation and degradation generates smaller plastics, commonly known, because of their size, as microplastics (MPs < 5 mm) and nanoplastics (NPs < 1 μm) (Wright et al., 2013; Singh and Sharma, 2008). Plastic fragments have been detected in coastal waters, oceans, polar waters and marginal seas (Cózar et al., 2014; de Lucia et al., 2014; Isobe et al., 2017; Lusher et al., 2015). Microplastics concentrations have reached up to 0.5 and 8.5 mg L^{-1} in the south Pacific gyre and the southern North Sea respectively (Eriksen et al., 2013; Dubaish and Liebezeit, 2013). A recent mathematical model from (Isobe et al. (2019)) estimated that there will be a two fold increase in the concentration of MPs in a subtropical convergence zone by 2030 (Isobe et al. (2019)).

Microplastics are available to a wide range of biota (> 172 species) and are included in food webs (Lusher et al., 2015). Bivalves are proposed as target group to determine the potential accumulation and effects of MPs and NPs (Canesi et al., 2012) due to: their sessile status, the fact that they are cosmopolitan organisms, the large seawater volumes which they filter and that they are consumed by humans, thus playing a role in the trophic transfer of MPs and NPs in food webs. MPs have been recorded in the population of *Mytilus galloprovincialis* in Galicia (NW of Spain) with 2.55 ± 2.80 of MPs per gram of mussel (Pablo Reguera and Viñas, 2019). The distribution of MPs and NPs in different tissues is relevant to assess the potential translocation of particles inside organisms, and therefore to understand the toxicological effects and transfer of MPs and NPs into food webs (Martin et al., 2003). (Von Moos et al. (2012)) demonstrated that 80 μm MPs could be accumulated on the surface of mussel gills and transferred along gill filament channels to the mouth and into the digestive gland where translocation into cells could occur. MPs were found in mussel intestinal lumen and epithelium and in the digestive tubules (Von Moos et al. (2012)). (González-Soto et al. (2019)) assessed the ingestion of 4.5 mm MPs in mussels. (Browne et al. (2008a)) evidenced the translocation of MPs (3 and 9.6 μm PS at 0.51 g·L^{-1}) to the *Mytilus edulis* hemolymph and their prevalence after 48 days inside hemocytes. Also, Al-Sid-Cheikh (Al-Sid-Cheikh et al., 2018) described the accumulation of nanoplastics according to size (24 and 250 nm and ^{14}C-radiolabeled) in *Pecten maximus* after 6 h. The autoradiography showed the accumulation of 250 nm NPs in the intestine, while 24 nm NPs were dispersed in the whole-body, possibly indicating some translocation across epithelial membranes, although translocation was not confirmed.

Particles at micro and nanoscale level are rapidly depurated from bivalves due to its capacity to filter high volume of water. However, there are evidences about a not completely depuration of particles, remaining a 10 % of the internalized MPs inside the mussels (Woods et al., 2018). Some of the negative effects cited in the literature are: feeding modification, reproductive disruption, offspring, pseudofaeces production, adherence to mantle and gills, histopathological damage, alteration in antioxidative and detoxification enzymes, downregulation in shell formation genes, embriotoxicity, neurotoxicity, formation of granulocytromas, alteration in immune and trophic transfer (Setälä et al., 2016; Sussarellu et al., 2016; Wegner et al., 2012; Farrell and Nelson, 2013; Cole and Galloway, 2015; Ward and Kach, 2009; Kolandhasamy et al., 2018; Paul-Pont et al., 2016; Avio et al., 2015a; Balbi et al., 2017a).

According to the review by (Ferreira et al. (2019)), the number of papers with the key words “microplastics”, “marine” and “effects” was 1699 papers, while “nanoplastics”, “marine” and “effects” was 20 papers. Despite the large amount of articles about MPs, only a few studies have addressed the effects of NPs. There are only a few contributions to the knowledge concerning bivalves and NPs (González-Soto et al., 2019; Al-Sid-Cheikh et al., 2018; Balbi et al., 2017b; Canesi et al., 2016; González-Fernández et al., 2018). (González-Fernández et al. (2018)) described the aggregation of spermatozoa at 100 mg L-1 of 100 nm PS COOH in *Crassostrea gigas*. The malformation of *Mytilus galloprovincialis* larvae was found when exposed to 50 nm of PS NH2; EC_{50}: 0.142 g·L^{-1} (Balbi et al., 2017a) and a reduction in *Mytilus edulis* filtration rate and reproduction fitness was associated to exposure to 100, 200, 300 mg $L^{-1}$of 30 nm PS NPs (Wegner et al., 2012). (Canesi et al. (2016), 2015a) described how 50 nm of PS-NH_2 decreased the phagocytosis and lysosome membrane stability, which increased the apoptotic process and extracellular oxygen radicals in hemocytes of *M. galloprovincialis*.

In the case of *M. galloprovincialis*, high mortalities due to infection have never been reported (Domeneghetti et al., 2014; Romero et al., 2014), most likely due to its complex and efficient innate immune system (Figueras et al., 2019). However, could the immune function of mussels be compromised when these organisms are exposed to NPs? Could these NPs, due to their nanoscale size, translocate to the cellular level of the immune system affecting the main functions of hemocytes? What would the main mechanisms of the immune system be to cope with two common inputs such as infection and exposure to plastics? In the present work the mussel *M. galloprovincialis* was used as the target organism for PS NPs exposure of different sizes (50 nm, 100 nm and 1 μm). Although the concentrations of PS NPs used in this work represent the highest environmental levels of total MPs floating on the surface of the gyres, where MPs are known to be concentrated, they allow us to assess the potential toxicological responses in Mediterranean mussels.. The goals of this work were: i) to describe the distribution of 10 mg L^{-1} NPs in different mussel tissues, ii) to reveal the endocytic pathway route of NPs and translocation of NPs into hemocytes and iii) to study the effects on the immune cells and the effects on resilience (ability of immune cells to recover functional capacity from a disturbance and return to its pre-disturbed state) after PS NPs exposure in a regular bacterial infection scenario.

2. Materials and methods

2.1. Primary and secondary characterization of PS NPs

The PS NPs used in this study were from Polyscience, Inc: non-fluorescent PS NPs of 50 nm (cat#08691), 100 nm (cat#00876) and 1 μm (cat#07310) and also fluorescent PS NPs with an ex/em: 488/520 nm; 50 nm (cat#17149-10), 100 nm Fluoresbrite ® (cat# 17150-10) and 1 μm (cat#17154-10). The fluorescence of the Fluoresbrite ® PS NPs was incorporated in the core of the particles and not in the surface coating to avoid changes in the interactions NPS-NPs and cells-NPs. These differences which were evidenced with the characterization of the particles were of the same magnitude for all different size of PS NPs; however the standard deviation was higher due to higher values in the polydispersity index (PDI). To make comparison between PS NPs sizes and stablish conclusions, the Fluoresbrite ® and non-fluorescent PS NPs were never mixed in the experimental design and development. Stock suspensions of PS NPs were prepared in ultrapure water before the experiments. Stocks were sonicated with a bath sonicator (UP 200S Dr. Hielscher GmbH) for 10 min with 500 Hz of frequency.

Particle size, shape and structure were analysed by Scanning Electron Microscopy (SEM; n:130 images), Transmission Electron Microscopy (TEM; n:130 images) and Fourier-transformed infrared spectroscopy (FTIR).

The size distribution and zeta potential were studied (at 0, 3 and 24 h) in the aqueous fluids [ultrapure water (MQ), filtered seawater

(FSW) and serum hemolymph (SH) filtered by 0.2 µm] to study agglomeration and deagglomeration of PS NPs processes. These measurements were performed using Dynamic Light Scattering; DLS (Zetasizer Nano ZS90, Malvern Instruments, equipped with software version 7.10) at 1 mg L^{-1}.

2.2. In vivo assays to study the bioaccumulation and translocation of PS NPs assays to study the bioaccumulation and translocation of PS NPs

M. galloprovincialis Lamarck specimens with a shell length and width of 3.63 ± 0.33 and 1.91 ± 0.34 cm, respectively, were collected at an unpolluted reference site: Cabo Home (Ría de Vigo, Galicia, NW Spain). For depuration and acclimation, the mussels were maintained in open-circuit filtered seawater tanks at 15 °C with aeration and fed daily with *Phaeodactylum tricornutum* and *Isochrysis galbana* over 2 weeks.

Four treatments were used for the experiments: control and Fluoresbrite ® 50 nm, 100, nm and 1 µm Ps NPs. Treatments with Fluoresbrite ® were tested to a concentration of 10 mg L^{-1} in triplicate. Mussels (n:4 per replicate for each treatment) were maintained in bottles of 300 mL with constant aeration and sampled for histological analysis at 3 and 24 h. Both sampling times were chosen to assess short term PS NPs internalization (3 h) and differences in the Fluoresbrite ® PS NPs internalization after 24 h.

2.2.1. Histological analysis

Mussels were fixed using Davidson's fixative solution for 24 h and then transferred to Davidson's solution. A single transverse cross-section (approximately 5 µm thick) was excised from each individual following the procedures outlined by Howard et al. (2004) (Howard et al., 2004). Tissues were placed in slides dehydrated, and embedded in paraffin. Then sections were mounted on slides and deparaffinised. Some sections were stained with hematoxylin and eosin and the others were stained with DAPI.

To study the translocation of Fluoresbrite ® PS NPs into the immune cells, fresh hemolymph was extracted from mussels exposed to PS NPs over 3 h. The 3 h sampling time was chosen to study the translocation of Fluoresbrite ® NPs into circulatory system. From our previous experience with other particles we consider this to be enough enough time to observe accumulation of Fluoresbrite ® PS NPs in different tissues of the mussels. These samples were analysed immediately to determine the presence of Fluoresbrite ® PS NPs inside the hemocytes or PS NPs circulating freely in hemolymph serum.

All samples were observed using a confocal microscope (Leica DM 5500Q, 10x and 20x objective). The images were processed employing the LAS-AF (Leica Application Suite Advanced Fluorescence). DAPI and Fluoresbrite ® PS NPs were studied with an excitation:emission of 405: 410 − 475 nm and 488:515 − 520 nm, respectively. Images of each replicate were analysed by Image J software. Intensity of fluorescence was relativized with the area analysed in the tissues of mussel and immune cells.

2.3. In vitro assay in mussel hemocytes assay in mussel hemocytes

Adult *M. galloprovincialis* specimens (large size: 6.5 ± 1 cm long and 3.2 ± 0.5 cm wide) were purchased from a commercial shellfish farm (Vigo, Galicia, Spain) and maintained in open-circuit filtered seawater tanks at 15 °C over 7 days. The mussels were fed daily with the same algae species as described above. Hemolymph was extracted from the posterior adductor muscle using a sterile 1 mL syringe with an 18 G1/2" needle.

2.3.1. Uptake pathway of PS NPs into mussel hemocytes

Internalization of Fluoresbrite ® PS NPs into hemocytes and the endocytic NPs pathways were studied by flow cytometry (Fac Scalibur, Laser of excitation 488 nm). Through flow cytometry the granulocyte cell subpopulation was identified by cell size (FSC) and complexity (SSC) on the logarithmic scale.

Four different hemolymph pools (1:1; hemolymph: 0.2 µm filtered seawater) from 30 individuals were used for these experiments. Internalization of Fluoresbrite ® PS NPs after 3 h of exposure was assayed by both fixing the concentration at 10 mg L^{-1} and the number of particles at $1.8{\cdot}10^{7}$ particles·mL^{-1}. This sampling time (3 h) was chosen after confirmation of internalization and translocation into circulatory systems of Fluoresbrite ® PS NPs.

After the study of internalization of Fluoresbrite ® PS NPs in hemocytes we studied the uptake pathway. The main routes of endocytosis were inhibited: the phagocytosis route was inhibited with cytochalasin-D at 5 µM, the caveolae route with genistein at 100 µM and clathrin mediated endocytosis route with Pitstop2 at 200 µM. The routes were studied both individually and in pairs (cytochalasin-D + genistein, cytochalasin-D + Pitstop2 and genistein + Pitstop2). All inhibitor stocks were prepared in DMSO, therefore DMSO was also added to the controls. The incubation with inhibitors was done during 1 h and before exposure to PS NPs. After incubation, the hemocytes were exposed to 10 mg L^{-1} of Fluoresbrite ® PS NPs for 1 h. The time of inhibitors incubation (1 h) and exposure to PS NPs after inhibition of endocytic routes (1 h) to avoid the potential cell damage due to the inhibitors used. All incubations were kept in darkness at 16 °C. The internalization of Fluoresbrite ® PS NPs was analysed as the percentage of granulocytes with internalized Fluoresbrite ® PS NPs with respect to the total population of granulocytes. This was analysed by flow cytometry though an FL1 detector.

2.3.2. Images of PS NPs internalization and actin structure in hemocytes

Hemocytes (in a relation 1:4; hemocytes:filtered seawater) were exposed to 10 mg L^{-1} of Fluoresbrite ® PS NPs over 3 h on coverslips. The cells were fixed with 4 % PFA, washed three times with PBS, and stained with Phalloidin-Alexa 635 (1:40 dilution) and DAPI to 1 µg·mL^{-1}. The preparations were photographed using a confocal microscope, a Leica DM5500Q (63x objective).

2.3.3. Colocation of PS NPs in lysosomes

Colocation of Fluoresbrite ® PS NPs in the lysosomes of the hemocytes was studied after 3 h of exposure with a ratio hemolymph:filtered seawater (1:4). LysoSensor Blue DND-167 (Invitrogen) at 1 µM was used to track acidic organelles, such as lysosomes. Lysosomes and Fluoresbrite ® PS NPs were assessed though confocal microscopy (20× objective) with a excitation:emission of 405: 410 − 475 nm and 488:515 − 520 nm respectively. Pearson correlation and Manders` coefficients of were calculated to analyse colocation between PS NPs and lysosomes with Image J software with the JACoP plugin (n:9).

2.3.4. Effects of a Vibrio splendidus infection on hemocytes after PS NP exposure through an in vitro approach

Hemocytes (in a relation 1:1; hemolymph:filtered seawater) were exposed to 10 mg L^{-1} of different-sized non-fluorescent PS NPs. After 3 h of PS NP exposure 4 groups were established: controls, hemocytes exposed to NPs, hemocytes exposed to $2{\cdot}10^{7}$ cells·mL^{-1} of *Vibrio splendidus* strain LGP32 (controls of bacterial infection) and hemocytes exposed to PS NPs and *V. splendidus*. The experiments were developed with four replicates consisting of different pools of hemolymph (in each pool at least 20 individuals were used).

The responses, such as the percentage of apoptotic cells, ROS and phagocytic capacity were analysed by flow cytometry. Apoptotic cells were studied using the Annexin V-FITC Apoptosis Detection Kit BioVision according to the manufacturer's instructions. Annexin V-FITC to detect phosphatidylserine in the outside layer of the cytoplastic membrane was recorded by an FL1 detector.

H_2O_2 was analysed using dihydrorhodamine 1, 2, 3 (DHR 123). The samples were incubated at a final concentration of 28.87 µM in darkness at room temperature for 60 min (Qin et al., 2008). The H_2O_2 present in the cells was measured by an FL1 detector [band pass (BP)

533/30 nm].

The phagocytic capacity was evaluated with 1 μm fluorescent beads. Samples were incubated with 10:1 (beads:hemocyte ratio). The incubation time was 2 h in darkness at 16 °C. Phagocytosis was analysed in granulocytes by the FL1 detector [band pass (BP) 533/30 nm].

2.3.5. Gene expression

RNA extraction was carried out from the hemocytes submitted to the different in vitro treatments using the Maxwell 16 LEV simplyRNA kit (Promega), following the supplier's protocol. After extraction, the concentration of RNA was measured by NanoDrop ND1000 spectrophotometer (NanoDrop Technologies). Finally, the cDNA was synthesised by reverse transcription from 100 ng of total RNA of each sample, using the NZY First-Strand cDNA Synthesis Kit (Nzytech) according to the protocol of the Kit.

Gene expression of the genes with a known immune function in the mussel, such as IRG1, Mytilin D and Myticin C, oxidative genes like DUOX and antioxidant genes, like UCP2, were studied by Real Time PCR (qPCR). 18S gen was used as housekeeping. Gene expression was analysed using a 7300 Real Time PCR System (Applied Biosystems). cDNA was diluted 1:1 and mixed with 0.5 μl of each primer (10 μM) and 12.5 μl of SYBR Green PCR master mix (Applied Byosystems) in a final reaction volume of 25 μl. The standard cycling conditions were 95 °C for 10 min, followed by 40 cycles of 95 °C for 15 s and 60 °C for 30 s. All reactions were performed as technical duplicates. The relative gene expression was calculated following the Pfaffl method (Pfaffl, 2001). Expression levels were normalized with respect to the 18S expression for each sample. The sequences of the primers are shown in **Table S1**.

All in vitro experiments were developed twice by cuatriplicate.

2.3.6. Motility of hemocytes during exposure to PS NPs

Motility of hemocytes was assessed by their velocity and accumulated distance. Hemocytes were exposed to 10 mg L^{-1} of Fluoresbrite ® PS NPs (1:20; Hemolymph:filtered seawater). For each size of PS NPs, nanoplastic treated hemocytes and their controls were always recorded in parallel. Pictures of hemocytes were recorded every 30 s over 3 h through an inverted microscope (Nikon ELIPSE 80i with 10x objective). A total of 361 images were recorded in each movie, and at least 40 cells were tracked by Image J software stablishing in each one the position (x,y) of hemocytes. The software Chemotaxis and Migration Tools from Ibidi was used to obtain the velocity and accumulated distance of each cell tracked. All experiments were repeated twice. The movies are downloadable as supplementary material. The analysis of hemocyte motility was developed followed Rioult et al. (2013) methods (Rioult et al., 2013).

2.4. Statistical analysis

Data are shown as average ± standard deviation. Statistical analysis was carried out using the IBM SPSS, statistics 23 program. A one-way ANOVA with a Bonferroni post hoc test was developed for each response measured (significant differences at $p < 0.05$). Levene tests were developed in all analyses to check homogeneity of the variance.

3. Results

3.1. Primary and secondary characterization of PS NPs

Primary characteristics were studied by analysis of nominal size through TEM and SEM and corroboration of materials by FTIR. The supplier's information was confirmed in our results (Fig. 1**, A and Figure S1**).

Secondary characterization was studied at time 0 by hydrodynamic radii and zeta potential in each culture media analysed (Fig. 1**, B**). DLS showed values close to nominal size in ultrapure water. In FSW, the agglomeration was immediate at time zero, all PS NPs were greater than the 1000 nm agglomerate size; in FSW the PDI was higher than in ultrapure water, particles of 1 μm showed the lowest PDI values and therefore the lowest agglomeration in this media. In SH, hydrodynamic radii of 50 nm, 100 nm and 1 μm PS NPs showed lower agglomeration with respect to the agglomeration in FSW and the PDI in SH was also lower. Zeta potential showed negative values for all PS NPs and in all exposure media. The values of zeta potential were more negative when particles were suspended in ultrapure water from -27.4 to -39.3 mV, in filtered seawater from -13.3 to -26.8 mV and serum of hemolymph from -8.6 to -9.6 mV. When the zeta potential is between -30 − 30 mV, the instability of the particles and therefore the agglomeration of the particles is higher. On the other hand, when the zeta potential is lower than -30 mV and higher than 30 mV the stability of particles is higher, this was plausible explanation for the behaviour of PS NPs suspended in ultrapure water.

The agglomeration of PS NPs in the different media was studied at 0, 3 and 24 h **(Figure S2, A, B and C)**. The agglomeration stage of the particles according to the culture media was different. In ultrapure water all PS NPs (except 100 nm PS NPs without fluorescence) showed the same peaks in their agglomeration. Agglomeration and deagglomeration processes were observed when 50 nm and 100 nm PS NPs were suspended in filtered seawater; however, the agglomeration stage in this culture media for 1 μm PS NPs was stable showing peaks with only little deviations. In hemolymph serum, the agglomeration and deagglomeration of particles was observed; however, the differences among times were lower than the differences found in in filtered seawater.

3.2. Bioaccumulation of PS NPs in tissues and hemocytes of M. galloprovincialis. In vivo assays

The agglomeration of non-fluorescent and Fluoresbrite® PS NPs was not the same. These differences which were evidenced with the characterization of the particles were of the same magnitude for all different size of PS NPs. In order to make comparison between PS NPs sizes and stablish conclusions, the Fluoresbrite ® and non-fluorescent PS NPs were never mixed in the experimental design and development. Fluoresbrite ® 50 nm, 100 nm and 1 μm Ps NPs were localized in the different tissues of mussels (Fig. 2**, A and B**). All PS NPs had a common destination; the digestive gland. From 3 h to 24 h of exposure, PS NPs were found in the stomach lumen, epithelia of the stomach and lumen of the digestive tubules (Fig. 2**, A and B**). More 1 μm particles were found in the digestive gland than those of 50 and 100 nm diameter after 24 h of exposure ($p < 0.05$); Fig. 2**, D**. The same trend for PS NP accumulation was found in the gills. PS NPs were less abundant in the gills than in the digestive gland. In all analyses, only once were 50 nm PS NPs found in the lumen of the gills after 24 h of exposure; however, in the remaining samples for 50 nm and 100 nm no Ps NPs were found in the gills. Among the particles tested, 1 μm PS NPs were the most abundant in the gills, although this presence of 1 μm PS NPs in the gills was much smaller than in the digestive gland. Large amounts of 1 μm PS NPs particles were found in the mucus (**Figure S3**) after 3 h of exposure to the plastics while 50 nm and 100 nm PS NPs were not. All PS NPs from 50 nm to 1 μm were showed in the muscle and feet of the mussels after 3 and 24 h; however, the presence was not significant ($p > 0.05$).

Translocation of PS NPs from tissues to cells was studied through the analysis of the hemolymph after 3 h of exposure to PS NPs (Fig. 2**, C and D**). After 3 h of PS NP exposure all the particles tested were found in the hemolymph (hemocytes and serum). Although all PS NPs were observed in the hemolymph, the translocation to hemocytes showed a size-dependent internalization. The smallest PS NPs (50 nm) were the most internalized particles by hemocytes ($p < 0.05$), followed by 100 nm and 1 μm. Particles of 50 nm, showed that most of the particles of 50 nm were found inside the hemocytes and they were not found in the surrounding serum of the hemolymph. On the other hand, the biggest PS NPs (1 μm) were often found in the hemolymph, whereas

A

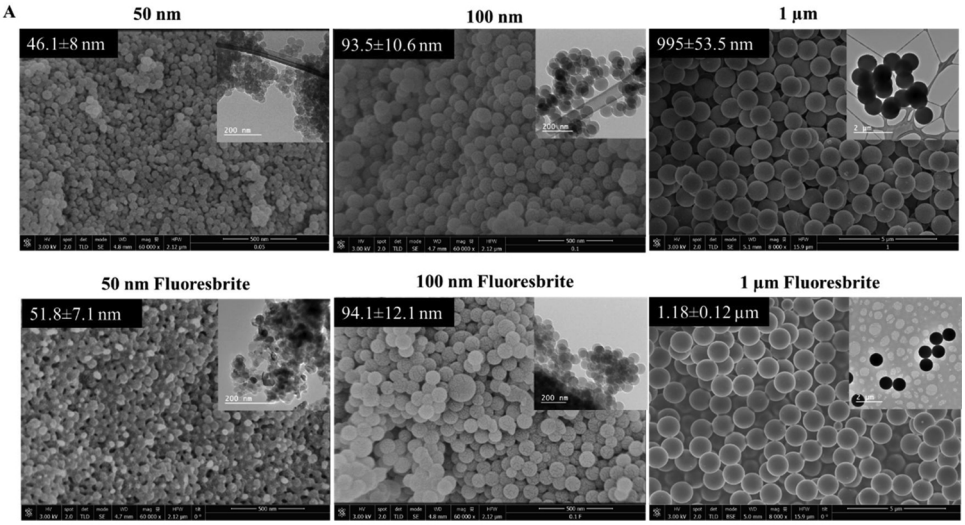

B

NPs	MQ			FSW			SH		
	Z-Avg. (nm) DLS	PDI	ζ (mV)	Z-Avg. (nm) DLS	PDI	ζ (mV)	mean	PDI	ζ (mV)
50 nm	54.2 ±17.7	0.07	-28.2	4086±591	0.30	-13.3	196.9±92.2	0.16	-9.6
50 nm F	64.2±15.6	0.02	-27.4	1032±144.6	0.64	-24.8	514.8±302.5	0.25	-9.3
100 nm	99.4±23.3	0.03	-28.8	1577±310.9	0.53	-18.4	276.6±124.3	0.23	-8.6
100 nm F	99.1±20.8	0.01	-34.7	1418±207.2	0.41	-26.7	368.4±186.3	0.21	-9.9
1 µm	1518±706.9	0.14	-39.3	1816±570.8	0.16	-26.8	1766±582.4	0.15	-9.4
1 µm F	1323±281.3	0.03	-35.7	2593±1103	0.15	-18.6	2000±1206	0.33	-9.1

Fig. 1. Primary and Secondary characterisation of the PS NPs tested. **Panel A**: SEM and TEM images (n:300), images of 50 nm, 100 nm and 1 µm without fluorescence were previosuly published in Sendra et al. (2019). **Panel B**: hydrodynamic radii, polydispersity index (PDI) and zeta potential (ζ) of the PS NPs by DLS in different culture media [ultrapure water (MQ), filtered seawater (FSW) and hemolymph serum (SH)] at time 0 h (n:3).

some particles were internalized by cells. Although 50 nm PS NPs were the particles most found inside the hemocytes, these particles were difficult to observe in histological images, and they were more abundant in the digestive gland (Fig. 2).

3.3. Internalization and endocytic pathways of PS NPs in mussel hemocytes. An in vitro approach

The internalization of different sizes of PS NPs was studied in the mussel granulocytes (Fig. 3, **A** and Fig. 4). The internalization studied according to concentration in 10 mg L^{-1}, 89.7 ± 1.9 % of granulocytes internalized the smallest PS NPs (50 nm) while the internalization rate for 100 nm and 1 µm PS NPs was of 60.6 ± 3.5 and 59.3 ± 5.3 %, respectively. When the same experiment was analysed considering the number of particles·mL^{-1} ($1.8{\cdot}10^7$ particles·ml^{-1}) this trend changed with values of 0.5 ± 0.1, 13.9 ± 27.4 and 52.5 ± 7.1 % of particles internalized for 50 nm, 100 nm and 1 µm PS NPs, respectively (Fig. 3, **A)**.

These data suggest the existence of different endocytic NP uptake routes in granulocytes according to their size (Fig. 3, **B** and Fig. 4). 50 nm PS NPs were internalized at rates of 93.7 ± 4.4 %; however, a significant reduction was found when the inhibitors genistein and pitstop2 were employed ($p < 0.05$). Hence internalization of 50 nm PS NPs decreased to 68.8 ± 5.7 % and 68.7 ± 7.3 % respectively. This decrease in the internalization of 50 nm PS NPs was more pronounced when the mixture of both inhibitors was tested, with an internalization of 54.9 ± 8.3 %.

With respect to 100 nm PS NPs, they were internalized by 56.6 ± 4.4 % of the granulocytes. All the inhibitors tested showed significant differences in the reduction of 100 nm PS NP uptake, values were observed of 38.5 ± 3.3, 22.6 ± 4.0 and 24.4 ± 3.7 for cytochalasin-D, genistein and Pitstop2, respectively (Fig. 3, **B**; $p < 0.05$). Genistein in combination with cytochalasin-D and pitstop2 showed a higher and significant reduction of 100 nm PS NP uptake, reaching up to 11.0 ± 1.7 and 11.8 ± 3.2 % respectively ($p < 0.05$).

According to the internalization of 1 µm PS NPs, values of 53.1 ± 12.4 % were found (Fig. 3, **B**). The three inhibitors showed a significant decrease in the internalization of the particles, with values of 35.5 ± 15.3, 27.2 ± 9.5 and 34.4 ± 6.8 % for cytochalasin-D, genistein and pitstop2 respectively ($p < 0.05$). In relation to the mix of inhibitors, an internalization value of 17.6 ± 2.43 % was found for Cytochalasin-D-genistein, 22.1 ± 1.5 % for cytochalasin-D-Pitstop2 and 20.2 ± 0.3% for genistein-Pitstop2 (Fig. 3, **B**).

3.4. Collocation of PS NPs with lysosomes

All sizes of PS NPs were internalized by the hemocytes with rates ranging from 90 to 59.3 % from the smallest to the highest PS NPs

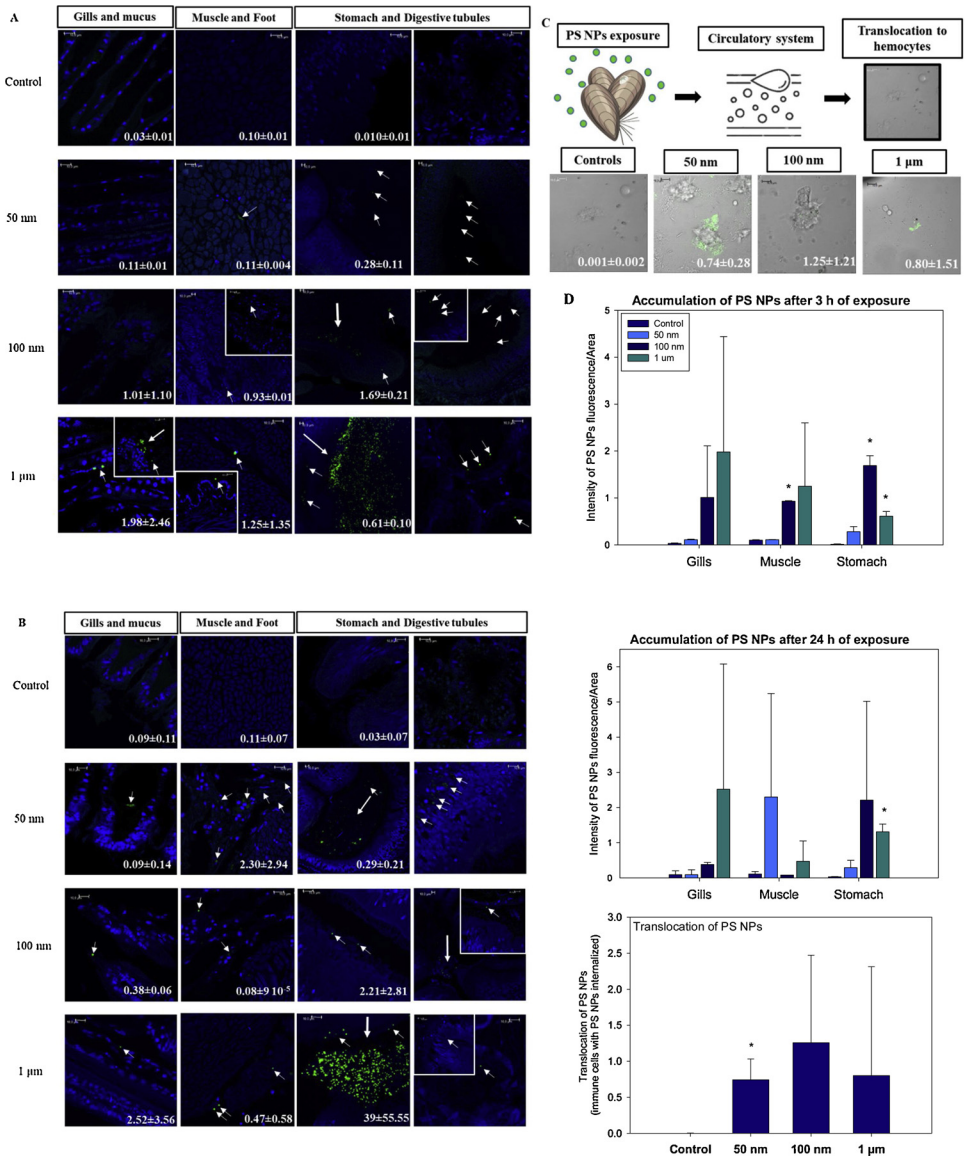

Fig. 2. Internalisation and translocation of Fluoresbrite ® PS NPs from tissue to the hemocytes. **Panels A** and **B** show the internalisation of PS NPs (10 mg L^{-1}) in the most representative tissues after 3 and 24 h of exposure respectively; blue and green colours indicate DAPI and fluorescence of PS NPs respectively (n:4), the scale bar is 10 µm. **Panel C** shows the translocation of PS NPs after 3 h of exposure to the plastics (n:4). **Panel D** shows the quantification of intensity of PS NP fluorescence with respect to the area analysed for accumulation of NPs in the different tissue and translocation experiments (n:4). ANOVA analysis and a Bonferroni Post hoc were performed; asterisks show significant differences between the controls and treatments ($p < 0.05$).

tested. When the collocation of PS NPs with lysosomes was studied, most of the particles regardless of their size were found in lysosomes; 0.66 ± 0.14, 0.71 ± 0.17 and 0.85 ± 0.11 for 50 nm, 100 nm and 1 µm PS NPs respectively (Fig. 3, **C and D**). However, 50 nm PS NPs showed a significantly lower collocation rate than 1 µm PS NPs ($p < 0.05$) and were found in the cytoplasm.

3.5. Motility of hemocytes exposed to PS NPs

Hemocyte motility was affected by PS NPs: hemocytes exposed to 50 nm PS NPs increased their velocity with respect to the controls for the 3 h analysed ($p < 0.001$) while the cells exposed to 1 µm decreased their velocity. The 100 nm PS NPs reduced the hemocytes' motility only over the first hour of exposure ($p < 0.001$). This trend was more pronounced in the third hour of exposure. The velocity of the controls was 2.3 ± 1.5 µm·min^{-1}, while the velocity of 50 nm, 100 nm and 1 µm PS NPs were 5.6 ± 1.5, 1.82 ± 1.5 and 0.4 ± 0.2 µm·min^{-1}, respectively (Fig. 5, **B**; $p < 0.05$).

Concerning the accumulated distance, the same trends were found when the hemocytes were exposed to the different PS NPs (Fig. 5, **A and B**). A significant increase of accumulated distance was observed for the hemocytes exposed to 50 nm PS NPs with respect to the controls over the three hours of exposure ($p < 0.001$). On the other hand, the accumulated distance of hemocytes was diminished when they were exposed to 1 µm PS NPs. The accumulated distance in the third hour of PS NPs exposure was for the controls 136.1 ± 93.6 µm and 324.1 ± 88.1, 106.0 ± 87.6 and 26.0 ± 15.2 µm for the hemocytes exposed to 50 nm, 100 nm and 1 µm PS NPs, respectively.

3.6. Infection with Vibrio splendidus in hemocytes previously exposed to PS NPs

After 3 h of exposure to PS NPs, an increase of the percentage of apoptotic cells with respect to the controls was only found when the granulocytes were exposed to 1 µm PS NPs: the hemocytes exposed to 1 µm PS NPs with levels of 25.9 ± 4.3 % versus 13.6 ± 1.9 % in the control ($p < 0.05$) and the hemocytes exposed to PS NPs + *V. splendidus* with a percentage of 35.6 ± 9.7 % versus values found in the *V. splendidus* controls 16.7 ± 2.1 % ($p < 0.05$). Although they showed significant differences with their controls, no significant differences were found between both conditions (Fig. 6).

A decrease in the percentage of ROS in the hemocytes was observed under the different treatments (Fig. 6). The hemocytes exposed to both conditions; PS NPs and PS NPs + *V. splendidus* showed the same pattern

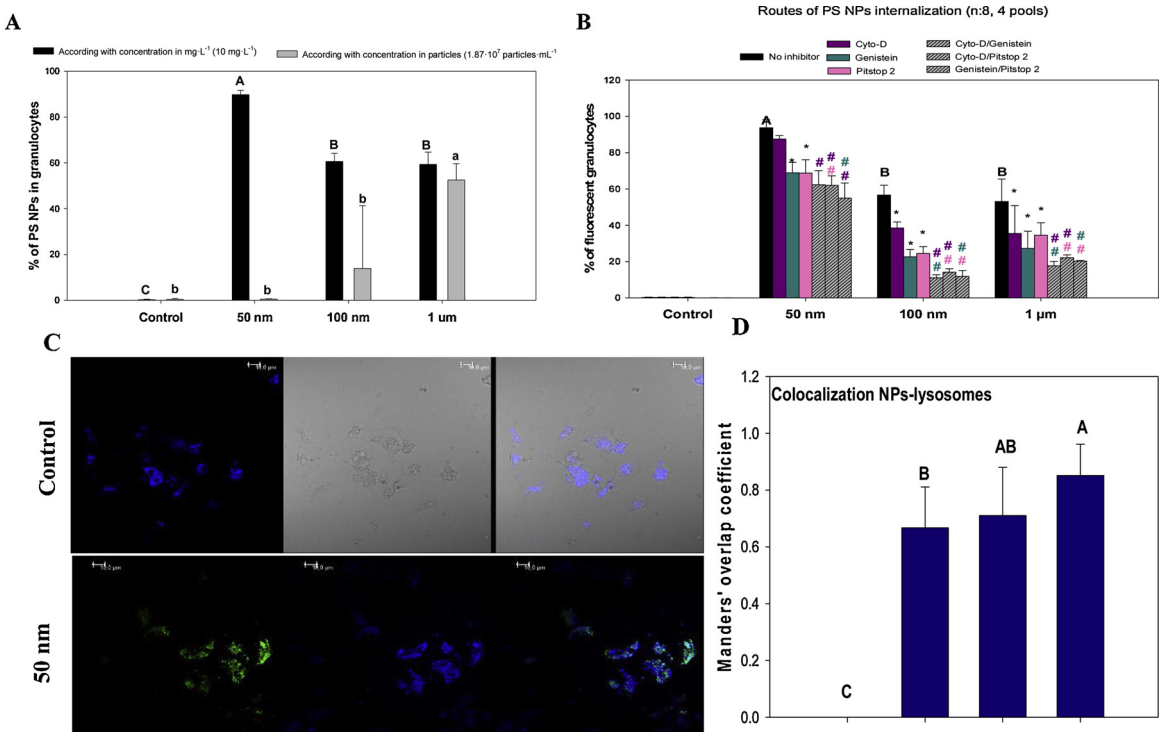

Fig. 3. Internalisation of Fluoresbrite ® PS NPs in the hemocytes after 3 h of exposure using an in vitro approach. **Panel A** shows the internalisation of PS NPs by granulocytes under exposure to PS NPs according to the concentration in $mg{\cdot}L^{-1}$ and $particles{\cdot}mL^{-1}$ (n:8). **Panel B** shows the endocytic routes of PS NP internalisation in the granulocytes. Endocytic routes such as phagocytosis, caveolae route and clathrin mediated endocitosis were inhibited by cytochalasin-D, genistein and Pitstop2 respectively (n:8). Pairs of inhibitors were used to inhibit several mechanisms of endocitosis at the same time. Uppercases show significant differences among PS NP treatments (50 nm, 100 nm and 1 µm), asterisks show significant differences between the internalisation of PS NPs without inhibitors and internalisation of PS NPs with inhibitors in single and combined forms and # shows significant differences in PS NP internalisation between single and combined inhibitors; colour indicates an inhibitor that it is statistically significant ($p < 0.05$). **Panel C** shows the co-localisation of PS NPs and lysosomes (blue: lysosomes and green: PS NPs). Images (n:4) were recorded with the same gain in the confocal microscope. **Panel D** shows Manders' overlap coefficient to measure the colocalization between Lysosomes and PS NPs (n:9), scale bar:10 µm. ANOVA analysis and a Bonferroni Post hoc were performed; uppercases indicate significant differences among treatments ($p < 0.05$).

with respect to the percentage in ROS levels. The hemocytes treated with 50 nm PS NPs showed a significant decrease of ROS levels (with values of 23.1 ± 4.8 %) with respect to the controls (33.5 ± 6.7 %; $p < 0.05$). A significant decrease in ROS levels was also found when the hemocytes were exposed to 100 nm and 1 µm PS NPs in combination with *V. splendidus*. A significant decrease was observed between the hemocytes exposed to 100 nm and 1 µm PS NPs + *V. splendidus* (30.7 ± 4.2 and 14.1 ± 6.1 % respectively) versus *V. splendidus* controls (44.8 ± 6.4 %; $p < 0.05$). Furthermore, significant differences were found between the ROS levels in the hemocytes under both conditions (exposed to 1 µm PS NPs, with and without infection).

The data concerning phagocytic capacity showed a significant decrease ($p < 0.05$) when the hemocytes were exposed to all the PS NPs tested but not when hemocytes were exposed to PS NPs + *V.splendidus* in combination (Fig. 6; $p < 0.05$). The data concerning phagocytic capacity showed a 60.0 ± 8.7 % of phagocytic cells in the controls with respect to 42.7 ± 2.9, 32.4 ± 1.4 and 36.1 ± 5.3 % for the cells exposed to 50 nm, 100 nm and 1 µm PS NPs respectively.

Concerning gene expression, Myticin C was the only one modulated by all the treatments. Myticin C showed a significant downregulation in its expression when the hemocytes were exposed to *V. splendidus* after 3 h exposure to 50 nm, 100 nm and 1 µm PS NPs (Fig. 6, $p < 0.05$) (Fig. 6). The other genes studied related to defensive functions such as IRG1, Mytilin D, and to oxidative mechanisms such as UCP2 and Duox did not show a significant modulation when the hemocytes were exposed to the different treatments (**see figure S4, Supplementary information**). IRG1 and Mytilin D showed an increase in their expression in some samples both without and with infection respectively when the hemocytes were exposed to 1 µm Ps NPs ($p > 0.05$). Regarding UCP2 and Duox no trend was found for any treatment and condition.

4. Discussion

The study of distribution of NPs in the different tissues of *M. galloprovincialis* will contribute to the assessment of potential translocation of NPs within an organism and, to the knowledge of any toxicological effects and NPs transfer in food webs. Small particles such as 50 nm and 100 nm PS NPs were more difficult to find in mussel tissues than 1 µm PS NPs however, the NP distribution in the different organs of the mussels was independent of their size. Most of the particles were found in the digestive gland while their numbers diminished in the muscle and gills. This NP distribution was in accordance with the study by (Al-Sid-Cheikh et al. (2018)), who observed a higher concentration of C^{14} PS NPs in the digestive gland of the scallop *Pecten maximus*, although the size of the NPs was (24 nm) and less in the gonads, muscle and gills. (González-Soto et al. (2019)) studied the distribution 4.5 µm MPs in different tissues of *M. galloprovincialis*. A greater internalization of MPs was also found in the stomach lumen and tubules of the digestive gland. Several other studies, as well as ours also support two uptake mechanisms i) the gill surface and ii) via the transference of MPs along the gill channels via cilia movement to the mouth and into the digestive gland (González-Soto et al. (2019); Paul-Pont et al., 2016; Avio et al., 2015b; Browne et al., 2008b; Magni et al., 2018; Pittura et al., 2018).

Our results show that the presence of PS NPs in the muscular tissue seems to be a characteristic occurrence at the nanoscale level. This has not been reported before in studies with MPs. The ubiquity of NPs in the

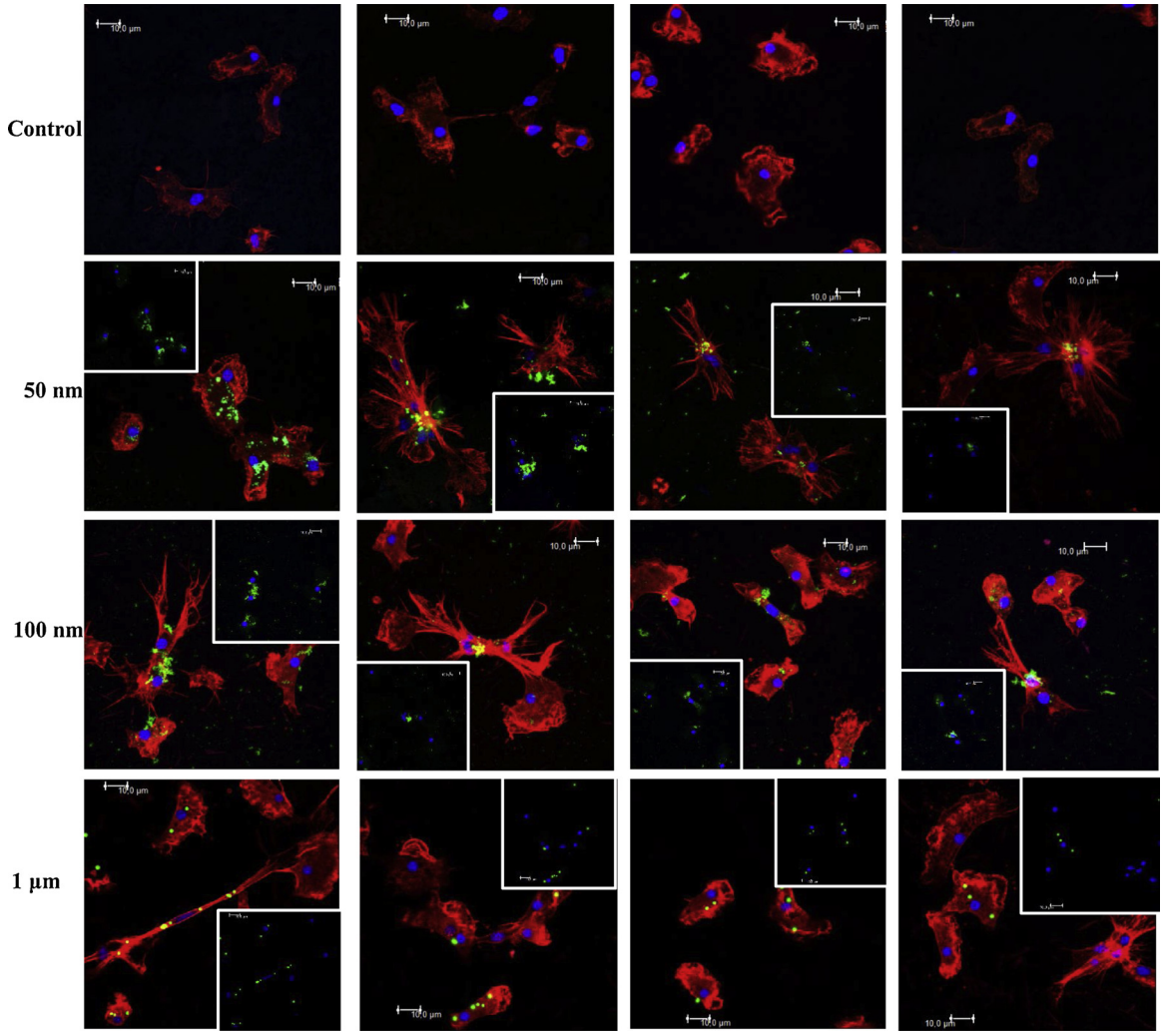

Fig. 4. Fluoresbrite ® PS NP internalisation and changes in actin conformation (blue: DAPI, red: actin and green:PS NPs), images were recorded with the same gain in the confocal microscope (n:4). Scale bar:10 µm.

muscle could indicate that they are able to cross the epithelial membrane, the cell membrane and lastly translocate into cells. Regarding the exposure to 1 µm PS NPs, a large amount of them were found in the mucus after 3 h. Among the functions of the mucus, one of them is the capture of food particles (Beninger et al., 2019). (Al-Sid-Cheikh et al. (2018)), proposed the translocation of NPs into the circulatory systems as they found NPs distributed throughout the whole body of the organism; however, this hypothesis was not supported experimentally. (Browne et al. (2008a)) described that hemocytes incorporated MPs (3 and 9.6 µm) in a size-dependent way after 12 h of MP exposure with a higher concentration than that of the environment. Our results show the translocation of NPs into the circulatory system after a very short time (3 h). All sizes of particles were found in the hemolymph. The internalization by hemocytes was higher for 50 nm PS NPs, while 1 µm PS NPs were found in the hemolymph with a higher volume of them present in the serum. Due to the open circulatory system in mussels and the higher translocation of 50 nm PS NPs, these particles could be the main candidate to reach the gonads and the hepatopancreas. In conclusion the translocation of NPs to hemocytes could increase the length of residence time, the ad/absorption by vital organs and unwanted effects in the mussels.

Once the translocation to hemocytes was confirmed, the study of the entry of PS NPs in hemocytes by a different energy-dependent endocytic pathway was a plausible goal. The internalization of PS NPs of different sizes was different when the concentration was used in terms of mass or in terms of particles. In terms of mass (10 mg L^{-1} for all PS NPs) the most internalized NPs were 50 nm followed by 100 nm and 1 µm. On the other hand, in terms of particles ($1.87 \cdot 10^{7}$ particles·mL^{-1}) the most internalized NPs were 1 µm followed by 100 nm and 50 nm. These results led to the hypothesis that small particles (50 nm) were being internalized by a different uptake route than those of 1 µm. To check this hypothesis, the most important endocytic routes were inhibited: (i) the phagocytic pathway; phagocytosis and ii) non-phagocytic pathways; macropynocytosis, caveolin-mediated endocitosis and clathrin-mediated endocytosis. The results showed that under simple and mixed endocytic inhibitors, the decrease in the internalization of 50 nm PS NPs in hemocytes did not reach 50 % (this decrease in the internalization of 50 nm PS NPs was only significant when the caveolae and clathrin routes were inhibited) while the addition of endocytic inhibitors decreased the uptake of 100 nm and 1 µm PS NPs by more than 50 %. The conclusion obtained from these results was that the uptake of 50 nm PS NPs is not governed by these classical endocytic routes.

The main fate of NPs is that they converge upon the lysosomes in the cells by endocytic routes; the function of the lysosomes is the sequestration and degradation of non-self materials. Metallic nanoparticles and oxide metallic nanoparticles, such as TiO_2, carbon, Ag, CeO_2 NPs; (Katsumiti et al., 2015; Jimeno-Romero et al., 2016, 2017; Sendra et al., 2018), lead to the instability of the lysosome membrane triggering cytosolic acidification, and therefore leading to the spoiling of cell organelles, ROS generation, mitochondrial damage, apoptotic and

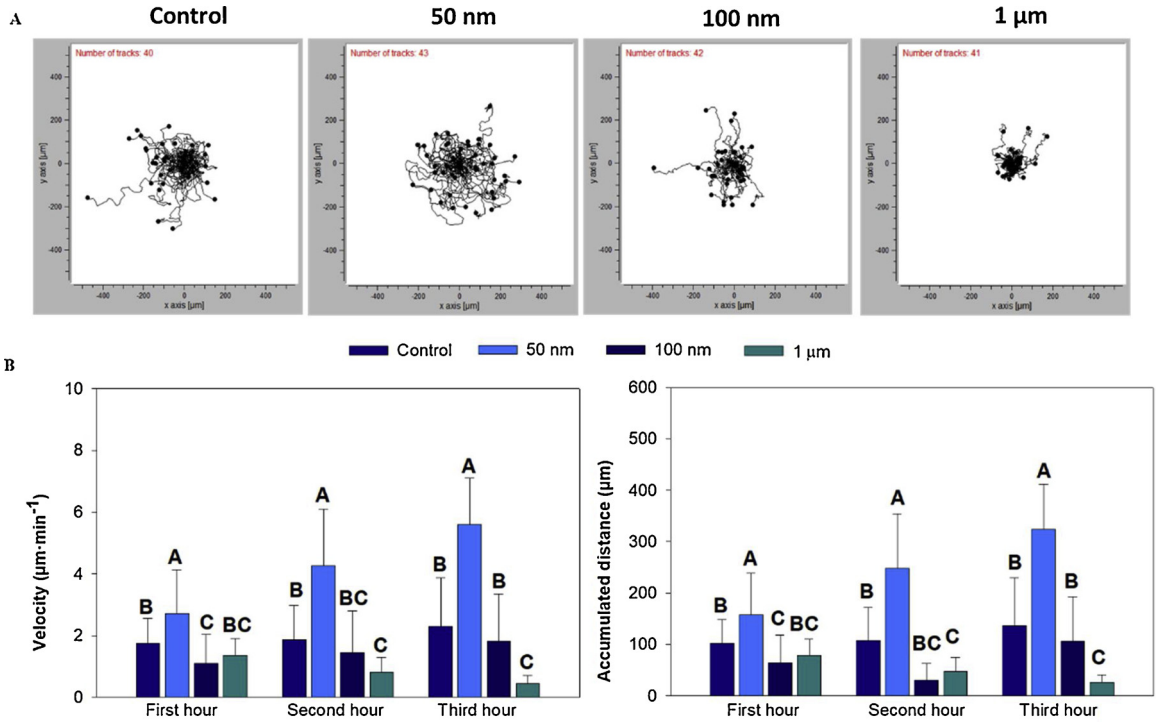

Fig. 5. Motility of hemocytes over 3 h of exposure to Fluoresbrite ® PS NPs. **Panel A** shows the tracks of each single cell analysed when it was exposed to PS NPs over three hours (at least 40 tracks were analysed in a total of 361 images). **Panel B** shows the velocity and accumulated distance of hemocytes exposed to PS NPs hour by hour. ANOVA analysis and a Bonferroni Post hoc were performed; uppercases indicate significant differences among treatments.

necrotic processes (He et al., 2016). (Canesi et al. (2015b)) described the lack of lysosome stability in *M. galloprovincialis* hemocytes when they were exposed to 50 nm NH_2 PS. Although most of the different sized NPs were found in the lysosomes, the 50 nm PS NPs were also found outside the lysosomes. This could indicate that different endocytic or non-endocytic pathways could be responsible for the internalization of 50 nm PS NPs. The uptake of the NPs by phagocytic and clathrin-mediated endocytosis led to phagosomes, clathrin-coated vesicle formation (endosomal). These endosomal compartments are fusioned with the lysosomes leading to non-self-material degradation (Stern et al., 2012). On the other hand, the caveolae endocytic route internalizes the non-self-materials by caveolin invaginations. The caveolin vesicle releases its contents to the endosomes that then convert into caveosomes. The caveosomes are able to separate from the lysosomes and are moved along the cytoskeleton to the endoplasmic reticulum and the Golgi complex (Stern et al., 2012). In our confocal

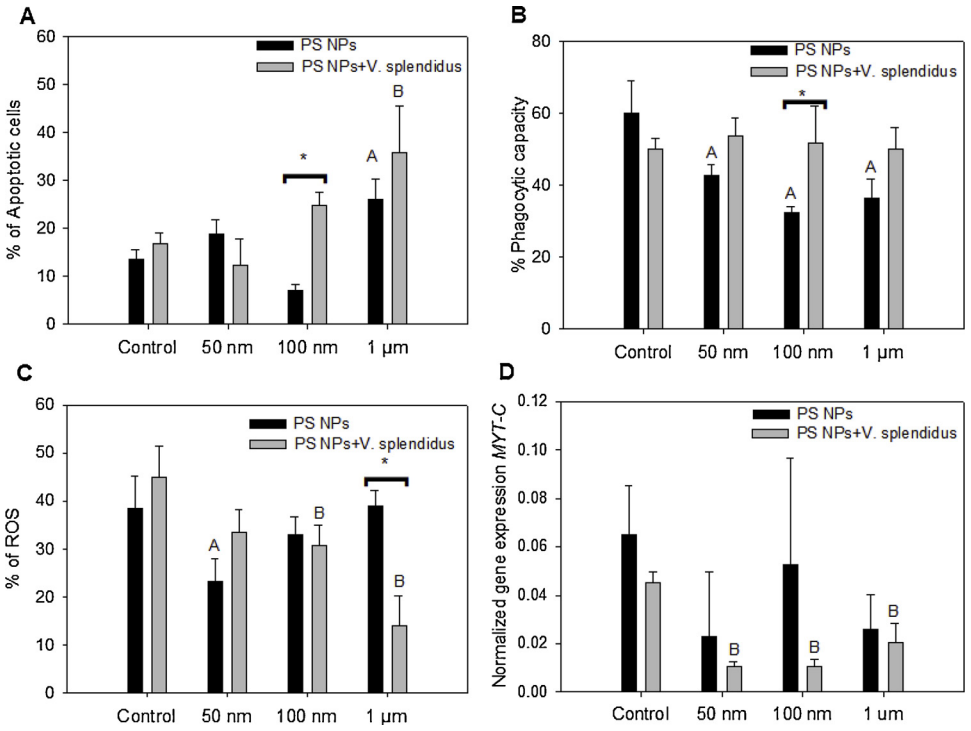

Fig. 6. Percentage of apoptotic cells (**panel A**), percentage of phagocytic capacity (**panel B**), percentage of ROS (**panel C**) and normalised myticin C gene expression (**panel D**) analysed in the hemocytes after 3 h after i) non-fluorescent PS NPs and ii) infection with *V. splendidus* after 3 h of non-fluorescent PS NP exposure. Uppercases A and B show significant differences among treatments within the same condition, only PS NPs and PS Nps + *V.splendidus* respectively. Asterisks show significant differences between conditions for the same treatment. $p < 0.05$; Bonferroni's post hoc test was performed.

images (Fig. 4), the internalization of 50 and 100 nm PS NPs was found in agglomerates and very close to the nucleus. Endoplasmic reticulum is usually around and nearby the nucleus, therefore, we hypothesized that the uptake of 50 and 100 nm PS NPs was internalized by the caveolae endocytic pathway. Furthermore, the inhibition of the caveolae route by genistein led to a lower internalization of the smaller NPs.

As explained before, actin is implicated in the uptake mechanics of endocytic pathways. The dynamic and remodelling of actin is involved in endosomal movements (Smythe and Ayscough, 2006). In the case of phagocytosis, the importance of actin in pseudopod extension and engulfment is well known; however, knowledge concerning the implications of actin in other endocytic routes is limited. (Doherty and McMahon (2009)) described that the clathrin coated vesicles are moved inside the cells with energy supplied by actin. In the present study, when hemocytes were exposed to 50 nm and 100 nm PS NPs the actin conformation was quite different with respect to the controls. This could indicate changes in actin conformation or cytoskeleton damage, however further studies are needed to fill this knowledge gap.

Once we knew that PS NPs are internalized by mussel tissues, translocated to the hemolymph and incorporated by the hemocytes, we determined their influence on hemocyte motility. Hemocytes are adherent cells with the ability to infiltrate tissues and migrate to infected and damaged zones (Costa et al., 2009). Assessing the motility of hemocytes is a technique that is very sensitive to environmental factors (Rioult et al., 2013). Our results showed that the activity of hemocytes was higher under 50 nm PS NP exposure, while the velocity and accumulated distance decreased when cells were exposed to 1 μm PS NPs. The velocity of mussel hemocytes (2.78 μm min^{-1}; (Rioult et al., 2013)) is similar to human extravascular neutrophils, 2.88 μm min^{-1} (Kreisel et al., 2010a), therefore mussel hemocytes are known to be strong motile cells. The fastest cells found in the work of Rioult et al. (2013) reached up to 7 μm min^{-1} similar to interstitial velocities reported for neutrophils at sites of inflammation (Kreisel et al., 2010b; Graham et al., 2009). The authors related this velocity to the activation of hemocytes due to an inflammatory response. (White et al. (2015)), found that iron oxide NPs also stimulated immune cells with an increase in the velocity of the microglia cells. As explained above, similar results in the increase of velocity were found in the present work when hemocytes were exposed to 50 nm PS NPs. On the other hand, hemocytes exposed to 1 μm PS NPs decreased their velocity, and therefore their activity.

Mussels are sessile filtering feeders that live in close contact with numerous marine pathogens but, unlike what happens in other bivalve species, their strong immune system prevents them from suffering major episodes of mortality (Domeneghetti et al., 2014; Romero et al., 2014; Gestal et al., 2008; Pezzati et al., 2015; Benabdelmouna et al., 2018). According to this premise and the motility results stated above, we wondered whether hemocyte activity triggered by PS NPs could compromise the cellular immune function when fighting against an infection. The hemocytes were exposed to PS NPs over 3 h, and then to *V. splendidus*. Changes in the percentage of apoptotic cells, ROS levels and phagocytic activity were determined when the hemocytes were exposed to the PS NPs; however, these values did not show additional effects when the hemocytes were infected with *V. splendidus*. A significant result was the lack of the phagocytic capacity of hemocytes when they were only exposed to PS NPs. However, when the hemocytes (previously exposed to PS NPs) were infected with *V. splendidus*, the phagocytic capacity was recovered, returning to phagocytic basal levels. Therefore, according to our results, it can be concluded that due to the resilience of hemocytes under an acute exposure to PS NPs followed by bacterial infection, the hemocytes were able to confront the infection having recovered their phagocytic capacity.

Concerning gene expression, Myticin C was the only gene analysed which was significantly modulated. Myticin C is a versatile and highly variable antimicrobial peptide associated to immune response and expressed in every development stage from larvae to adult mussel (Pallavicini et al., 2008). It has very diverse functions including antibacterial and antiviral activity and it can even regulate the immune response in a cytokine-similar way (Balseiro et al., 2011; Martinez-Lopez et al., 2013; Novoa et al., 2016). Myticin C expression has been recently found to be regulated in response to signals reporting damage, the gene is over-expressed in order to produce new AMPs, presumably as a preparation for a possible infection. However, its regulation at a transcriptomic level is not that evident for the case of bacterial infections, probably because of the reserves of AMPs that mussels already keep inside the granulocytes so that they can direct them immediately against an infection (Rey-Campos et al., 2019). In the present work, Myticin C expression showed significant differences between both conditions: PS NP treatments and PS NPs plus *V.splendidus* for all the NP sizes tested. A significant reduction in Myticin C gene expression was found when hemocytes were exposed to PS NPs plus *V. splendidus* in combination, with respect to its expression when the hemocytes were only exposed to NPs or only bacteria. This supposes a new effect of the impact that nanoplastics have when translocating to the interior of the defensive cells, which is that they are able to compromise their function.

Chronic exposure under real scenarios is a new challenge for marine fauna, especially filter feeders, of which *Mytilus galloprovincialis* is one of the most representative species. Unfortunately, there are technical limitations to determine the real nanoplastic concentrations in oceans. The concentrations of PS NPs used in this work represent the highest environmental levels of total MPs floating on the surface of the gyres. Since there is a lack of information on the potential negative effects of nanoplastics under real scenarios such as bacterial infection, climate change or pollutant environments we used these high concentrations to increase our knowledge on the effect of different PS NPs on mussel immune response because.

5. Conclusions

Mussel digestive gland was the tissue that most accumulates 50 nm, 100 nm and 1 μm PS NPs exposure. Muscle was another tissue where the three particles tested for were found; mainly for smaller particles (50 and 100 nm) as a great amount of 1 μm PS NPs were associated to the mucus.

The immediate translocation of PS NPs into hemocytes was confirmed, as well as the main uptake routes. The mediated endocytic route was the principal mechanism to uptake larger particles (100 nm and 1 μm) in the hemocytes, while the internalization of the smallest particles (50 nm) did not reach an inhibition of at least 50 % by any endocytic mechanism. Therefore, the authors suggest that endocytic and non-endocytic pathways are both responsible for the internalization of 50 nm Ps NPs.

The NP uptake pathways could be key to hemocyte motility. The internalization of NPs within the hemocytes triggered changes in the immune response such as motility, apoptosis, ROS and phagocytic capacity; however, these responses were not exacerbated under infection with *V. splendidus*. Even the hemocytes were able, in this case, to recover their phagocytic capacity. The effect of nanoplastics combined with a bacterial infection with *V. splendidus* had effects in gene expression, causing a modulation of Myticin C, which was not observed when treating either only with nanoplastics or only with bacterial infection.

Further studies are needed in this field, since this behaviour may be different under chronic exposure to NPs due to the long residence time that NPs can have in the organisms because of the translocation of the NPs.

Declaration of Competing Interest

The authors declare that they have no known competing financial interests or personal relationships that could have appeared to influence the work reported in this paper.

CRediT authorship contribution statement

M. Sendra: Investigation, Writing - original draft. **A. Saco:** Investigation. **M.P. Yeste:** Investigation. **A. Romero:** Investigation. **B. Novoa:** Methodology, Supervision. **A. Figueras:** Writing - review & editing, Conceptualization, Supervision.

Acknowledgements

This work was conducted with the support of the projects RTI2018-095997-B-I00 (Ministerio de Ciencia, Innovación y Universidades, Spain) and VIVALDI (678589) (EU H2020). M. Sendra and P. Yeste are grateful to CEI·MAR for their support through CEIJ-C06.1 and CEIJ-C06.2 projects. MS also wants to acknowledge the Spanish Ministerio de Ciencia, Innovación y Universidades for her Juan de la Cierva contract (TJFI-2017-32493). We acknowledge support for the publication fee by the CSIC Open Access Publication Support Initiative through its Unit of Information Resources for Research (URICI) and Consellería de Economía, Emprego e Industria (GAIN), Xunta de Galicia (IN607B 2019/01).

Appendix A. Supplementary data

Supplementary material related to this article can be found, in the online version, at doi:https://doi.org/10.1016/j.jhazmat.2019.121788.

References

PlasticsEurope, 2018. Plastics – the Facts. pp. 59. https://www.plasticseurope.org/application/files/6315/4510/9658/Plastics_the_facts_2018_AF_web.pdf.

Salvador Cesa, F., Turra, A., Baruque-Ramos, J., 2017. Synthetic fibers as microplastics in the marine environment: a review from textile perspective with a focus on domestic washings. Sci. Total Environ. 598, 1116–1129. https://doi.org/10.1016/j.scitotenv.2017.04.172.

Browne, M.A., 2008. Environmental consequences of microplastic inmarine habitats. No Title. Plymouth.

Alimi, O.S., Farner Budarz, J., Hernandez, L.M., Tufenkji, N., 2018. Microplastics and nanoplastics in aquatic environments: aggregation, deposition, and enhanced contaminant transport. Environ. Sci. Technol. 52, 1704–1724. https://doi.org/10.1021/acs.est.7b05559.

Wright, S.L., Thompson, R.C., Galloway, T.S., 2013. The physical impacts of microplastics on marine organisms: a review. Environ. Pollut. https://doi.org/10.1016/j.envpol.2013.02.031.

Singh, B., Sharma, N., 2008. Mechanistic implications of plastic degradation. Polym. Degrad. Stab. 93, 561–584. https://doi.org/10.1016/j.polymdegradstab.2007.11.008.

Cózar, A., Echevarría, F., González-Gordillo, J.I., Irigoien, X., Ubeda, B., Hernández-León, S., Palma, A.T., Navarro, S., García-de-Lomas, J., Ruiz, A., Fernández-de-Puelles, M.L., Duarte, C.M., 2014. Plastic debris in the open ocean. Proc. Natl. Acad. Sci. U. S. A. 111, 10239–10244. https://doi.org/10.1073/pnas.1314705111.

de Lucia, G.A., Caliani, I., Marra, S., Camedda, A., Coppa, S., Alcaro, L., Campani, T., Giannetti, M., Coppola, D., Cicero, A.M., Panti, C., Baini, M., Guerranti, C., Marsili, L., Massaro, G., Fossi, M.C., Matiddi, M., 2014. Amount and distribution of neustonic micro-plastic off the western Sardinian coast (Central-Western Mediterranean Sea). Mar. Environ. Res. 100, 10–16. https://doi.org/10.1016/j.marenvres.2014.03.017.

Isobe, A., Uchiyama-Matsumoto, K., Uchida, K., Tokai, T., 2017. Microplastics in the Southern Ocean. Mar. Pollut. Bull. 114, 623–626. https://doi.org/10.1016/j.marpolbul.2016.09.037.

Lusher, A.L., Tirelli, V., O'Connor, I., Officer, R., 2015. Microplastics in Arctic polar waters: the first reported values of particles in surface and sub-surface samples. Sci. Rep. 5, 1–9. https://doi.org/10.1038/srep14947.

Eriksen, M., Mason, S., Wilson, S., Box, C., Zellers, A., Edwards, W., Farley, H., Amato, S., 2013. Microplastic pollution in the surface waters of the Laurentian Great Lakes. Mar. Pollut. Bull. 77, 177–182. https://doi.org/10.1016/j.marpolbul.2013.10.007.

Dubaish, F., Liebezeit, G., 2013. Suspended microplastics and black carbon particles in the Jade system, southern North Sea. Water Air Soil Pollut. 224. https://doi.org/10.1007/s11270-012-1352-9.

Isobe, A., Iwasaki, S., Uchida, K., Tokai, T., 2019. Abundance of non-conservative microplastics in the upper ocean from 1957 to 2066. Nat. Commun. 10, 1–3. https://doi.org/10.1038/s41467-019-08316-9.

Canesi, L., Ciacci, C., Fabbri, R., Marcomini, A., Pojana, G., Gallo, G., 2012. Bivalve molluscs as a unique target group for nanoparticle toxicity. Mar. Environ. Res. 76, 16–21. https://doi.org/10.1016/J.MARENVRES.2011.06.005.

Pablo Reguera, J.G., Viñas, Lucía, 2019. Microplastics in wild mussels (*Mytilus* spp.) from the north coast of Spain. Sci. Mar. 83 (4) 83(4): 000–000.

Martin, J.W., Mabury, S.A., Solomon, K.R., Muir, D.C.G., 2003. Bioconcentration and tissue distribution of perfluorinated acids in rainbow trout (*Oncorhynchus mykiss*). Environ. Toxicol. Chem. 22, 196–204. http://www.ncbi.nlm.nih.gov/pubmed/12503765.

Von Moos, N., Burkhardt-Holm, P., Köhler, A., 2012. Uptake and effects of microplastics on cells and tissue of the blue mussel Mytilus edulis L. After an experimental exposure. Environ. Sci. Technol. 46, 11327–11335. https://doi.org/10.1021/es302332w.

González-Soto, N., Hatfield, J., Katsumiti, A., Duroudier, N., Lacave, J.M., Bilbao, E., Orbea, A., Navarro, E., Cajaraville, M.P., 2019. Impacts of dietary exposure to different sized polystyrene microplastics alone and with sorbed benzo[a]pyrene on biomarkers and whole organism responses in mussels *Mytilus galloprovincialis*. Sci. Total Environ. 684, 548–566. https://doi.org/10.1016/J.SCITOTENV.2019.05.161.

Browne, M.A., Dissanayake, A., Galloway, T.S., Lowe, D.M., Thompson, R.C., 2008a. Ingested microscopic plastic translocates to the circulatory system of the mussel, *Mytilus edulis* (L.). Environ. Sci. Technol. 42, 5026–5031. https://doi.org/10.1021/es800249a.

Al-Sid-Cheikh, M., Rowland, S.J., Stevenson, K., Rouleau, C., Henry, T.B., Thompson, R.C., 2018. Uptake, whole-body distribution, and depuration of nanoplastics by the scallop *Pecten maximus* at environmentally realistic concentrations. Environ. Sci. Technol. 52, 14480–14486. https://doi.org/10.1021/acs.est.8b05266.

Woods, M.N., Stack, M.E., Fields, D.M., Shaw, S.D., Matrai, P.A., 2018. Microplastic fiber uptake, ingestion, and egestion rates in the blue mussel (*Mytilus edulis*). Mar. Pollut. Bull. 137, 638–645. https://doi.org/10.1016/j.marpolbul.2018.10.061.

Setälä, O., Norkko, J., Lehtiniemi, M., 2016. Feeding type affects microplastic ingestion in a coastal invertebrate community. Mar. Pollut. Bull. 102, 95–101. https://doi.org/10.1016/J.MARPOLBUL.2015.11.053.

Sussarellu, R., Suquet, M., Thomas, Y., Lambert, C., Fabioux, C., Pernet, M.E.J., Le Goïc, N., Quillien, V., Mingant, C., Epelboin, Y., Corporeau, C., Guyomarch, J., Robbens, J., Paul-Pont, I., Soudant, P., Huvet, A., 2016. Oyster reproduction is affected by exposure to polystyrene microplastics. Proc. Natl. Acad. Sci. 113, 2430–2435. https://doi.org/10.1073/pnas.1519019113.

Wegner, A., Besseling, E., Foekema, E.M., Kamermans, P., Koelmans, A.A., 2012. Effects of nanopolystyrene on the feeding behavior of the blue mussel (*Mytilus edulis* L.). Environ. Toxicol. Chem. 31, 2490–2497. https://doi.org/10.1002/etc.1984.

Farrell, P., Nelson, K., 2013. Trophic level transfer of microplastic: *mytilus edulis* (L.) to *Carcinus maenas* (L.). Environ. Pollut. 177, 1–3. https://doi.org/10.1016/j.envpol.2013.01.046.

Cole, M., Galloway, T.S., 2015. Ingestion of nanoplastics and microplastics by pacific oyster larvae. Environ. Sci. Technol. 49, 14625–14632. https://doi.org/10.1021/acs.est.5b04099.

Ward, J.E., Kach, D.J., 2009. Marine aggregates facilitate ingestion of nanoparticles by suspension-feeding bivalves. Mar. Environ. Res. 68, 137–142. https://doi.org/10.1016/j.marenvres.2009.05.002.

Kolandhasamy, P., Su, L., Li, J., Qu, X., Jabeen, K., Shi, H., 2018. Adherence of microplastics to soft tissue of mussels: a novel way to uptake microplastics beyond ingestion. Sci. Total Environ. 610–611, 635–640. https://doi.org/10.1016/j.scitotenv.2017.08.053.

Paul-Pont, I., Lacroix, C., González Fernández, C., Hégaret, H., Lambert, C., Le Goïc, N., Frère, L., Cassone, A.-L., Sussarellu, R., Fabioux, C., Guyomarch, J., Albentosa, M., Huvet, A., Soudant, P., 2016. Exposure of marine mussels *Mytilus* spp. To polystyrene microplastics: toxicity and influence on fluoranthene bioaccumulation. Environ. Pollut. 216, 724–737. https://doi.org/10.1016/J.ENVPOL.2016.06.039.

Avio, C.G., Gorbi, S., Regoli, F., 2015a. Experimental development of a new protocol for extraction and characterization of microplastics in fish tissues: first observations in commercial species from Adriatic Sea. Mar. Environ. Res. 111, 18–26. https://doi.org/10.1016/J.MARENVRES.2015.06.014.

Balbi, T., Camisassi, G., Montagna, M., Fabbri, R., Franzellitti, S., Carbone, C., Dawson, K., Canesi, L., 2017a. Impact of cationic polystyrene nanoparticles (PS-NH2) on early embryo development of *Mytilus galloprovincialis*: effects on shell formation. Chemosphere 186, 1–9. https://doi.org/10.1016/j.chemosphere.2017.07.120.

Ferreira, I., Venâncio, C., Lopes, I., Oliveira, M., 2019. Nanoplastics and marine organisms: What has been studied? Environ. Toxicol. Pharmacol. 67, 1–7. https://doi.org/10.1016/j.etap.2019.01.006.

Balbi, T., Camisassi, G., Montagna, M., Fabbri, R., Franzellitti, S., Carbone, C., Dawson, K., Canesi, L., 2017b. Impact of cationic polystyrene nanoparticles (PS-NH2) on early embryo development of *Mytilus galloprovincialis*: effects on shell formation. Chemosphere 186, 1–9. https://doi.org/10.1016/j.chemosphere.2017.07.120.

Canesi, L., Ciacci, C., Fabbri, R., Balbi, T., Salis, A., Damonte, G., Cortese, K., Caratto, V., Monopoli, M.P., Dawson, K., Bergami, E., Corsi, I., 2016. Interactions of cationic polystyrene nanoparticles with marine bivalve hemocytes in a physiological environment: role of soluble hemolymph proteins. Environ. Res. 150, 73–81. https://doi.org/10.1016/j.envres.2016.05.045.

González-Fernández, C., Tallec, K., Le Goïc, N., Lambert, C., Soudant, P., Huvet, A., Suquet, M., Berchel, M., Paul-Pont, I., 2018. Cellular responses of Pacific oyster (*Crassostrea gigas*) gametes exposed in vitro to polystyrene nanoparticles. Chemosphere 208, 764–772. https://doi.org/10.1016/j.chemosphere.2018.06.039.

Canesi, L., Ciacci, C., Bergami, E., Monopoli, M.P., Dawson, K.A., Papa, S., Canonico, B., Corsi, I., 2015a. Evidence for immunomodulation and apoptotic processes induced by cationic polystyrene nanoparticles in the hemocytes of the marine bivalve *Mytilus*. Mar. Environ. Res. 111, 34–40. https://doi.org/10.1016/j.marenvres.2015.06.008.

Domeneghetti, S., Varotto, L., Civettini, M., Rosani, U., Stauder, M., Pretto, T., Pezzati, E., Arcangeli, G., Turolla, E., Pallavicini, A., Venier, P., 2014. Mortality occurrence and pathogen detection in *Crassostrea gigas* and *Mytilus galloprovincialis* close-growing in shallow waters (Goro lagoon, Italy). Fish Shellfish Immunol. 41, 37–44. https://doi.org/10.1016/j.fsi.2014.05.023.

Romero, A., Del Mar Costa, M., Forn-Cuni, G., Balseiro, P., Chamorro, R., Dios, S., Figueras, A., Novoa, B., 2014. Occurrence, seasonality and infectivity of Vibrio strains

in natural populations of mussels *Mytilus galloprovincialis*. Dis. Aquat. Organ. 108, 149–163. https://doi.org/10.3354/dao02701.
Figueras, A., Moreira, R., Sendra, M., Novoa, B., 2019. Genomics and immunity of the Mediterranean mussel *Mytilus galloprovincialis* in a changing environment. Fish Shellfish Immunol. 90, 440–445. https://doi.org/10.1016/j.fsi.2019.04.064.
Howard, D.W., Lewis, E.J., Keller, B.J., Smith, C.S., 2004. Histological Techniques for Marine Bivalve Mollusks and Crustaceans. NOAA Technical Memorandum NOS NCCOS 5, NOAA Tech. Memo. NOS NCCOS 5. pp. 218.
Qin, Y., Lu, M., Gong, X., 2008. Dihydrorhodamine 123 is superior to 2,7-dichlorodihydrofluorescein diacetate and dihydrorhodamine 6G in detecting intracellular hydrogen peroxide in tumor cells. Cell Biol. Int. 32, 224–228. https://doi.org/10.1016/j.cellbi.2007.08.028.
Pfaffl, M.W., 2001. A new mathematical model for relative quantification in real-time RT-PCR. Nucleic Acids Res. 29 (9) e45-e45.
Rioult, D., Lebel, J.M., Le Foll, F., 2013. Cell tracking and velocimetric parameters analysis as an approach to assess activity of mussel (*Mytilus edulis*) hemocytes in vitro. Cytotechnology 65, 749–758. https://doi.org/10.1007/s10616-013-9558-2.
Avio, C., Gorbi, S., F.R.-M, 2015b. Experimental development of a new protocol for extraction and characterization of microplastics in fish tissues: first observations in commercial species from Adriatic. Mar. Environ. Res. 111, 18–26.
Browne, M.A., Dissanayake, A., Galloway, T.S., Lowe, D.M., Thompson, R.C., 2008b. Ingested microscopic plastic translocates to the circulatory system of the mussel, *Mytilus edulis* (L.) BT. Environ. Sci. Technol. 42, 5026–5031.
Magni, S., Gagné, F., André, C., Della Torre, C., Auclair, J., Hanana, H., Parenti, C.C., Bonasoro, F., Binelli, A., 2018. Evaluation of uptake and chronic toxicity of virgin polystyrene microbeads in freshwater zebra mussel *Dreissena polymorpha* (Mollusca: bivalvia). Sci. Total Environ. 631–632, 778–788. https://doi.org/10.1016/j.scitotenv.2018.03.075.
Pittura, L., Avio, C.G., Giuliani, M.E., d'Errico, G., Keiter, S.H., Cormier, B., Gorbi, S., Regoli, F., 2018. Microplastics as vehicles of environmental pahs to marine organisms: combined chemical and physical hazards to the mediterranean mussels, *Mytilus galloprovincialis*. Front. Mar. Sci. 5, 103. https://doi.org/10.3389/fmars.2018.00103.
Beninger, P.G., St-Jean, S., Poussart, Y., Ward, J.E., 2019. Gill function and mucocyte distribution in *Placopecten magellanicus* and *Mytilus edulis* (Mollusca: bivalvia): the role of mucus in particle transport. Mar. Ecol. Prog. Ser. 98, 275–282. https://doi.org/10.2307/24833817. (n.d.).
Katsumiti, A., Gilliland, D., Arostegui, I., Cajaraville, M.P., 2015. Mechanisms of toxicity of Ag nanoparticles in comparison to bulk and ionic Ag on mussel hemocytes and gill cells. PLoS One 10, 1–20. https://doi.org/10.1371/journal.pone.0129039.
Jimeno-Romero, A., Oron, M., Cajaraville, M.P., Soto, M., Marigómez, I., 2016. Nanoparticle size and combined toxicity of TiO 2 and DSLS (surfactant) contribute to lysosomal responses in digestive cells of mussels exposed to TiO 2 nanoparticles. Nanotoxicology. 10, 1168–1176. https://doi.org/10.1080/17435390.2016.1196250.
Jimeno-Romero, A., Bilbao, E., Izagirre, U., Cajaraville, M.P., Marigómez, I., Soto, M., 2017. Digestive cell lysosomes as main targets for Ag accumulation and toxicity in marine mussels, *Mytilus galloprovincialis*, exposed to maltose-stabilised Ag nanoparticles of different sizes. Nanotoxicology. 11, 168–183. https://doi.org/10.1080/17435390.2017.1279358.
Sendra, M., Volland, M., Balbi, T., Fabbri, R., Yeste, M.P., Gatica, J.M., Canesi, L., Blasco, J., 2018. Cytotoxicity of CeO 2 nanoparticles using in vitro assay with *Mytilus galloprovincialis* hemocytes: relevance of zeta potential, shape and biocorona formation. Aquat. Toxicol. 200, 13–20. https://doi.org/10.1016/j.aquatox.2018.04.011.
He, H., Zheng, N., Song, Z., Kim, K.H., Yao, C., Zhang, R., Zhang, C., Huang, Y., Uckun, F.M., Cheng, J., Zhang, Y., Yin, L., 2016. Suppression of hepatic inflammation via systemic sirna delivery by membrane-disruptive and endosomolytic helical polypeptide hybrid nanoparticles. ACS Nano 10, 1859–1870. https://doi.org/10.1021/acsnano.5b05470.
Canesi, L., Ciacci, C., Bergami, E., Monopoli, M.P., Dawson, K.A., Papa, S., Canonico, B., Corsi, I., 2015b. Evidence for immunomodulation and apoptotic processes induced by cationic polystyrene nanoparticles in the hemocytes of the marine bivalve *Mytilus*. Mar. Environ. Res. 111, 34–40. https://doi.org/10.1016/j.marenvres.2015.06.008.
Stern, S.T., Adiseshaiah, P.P., Crist, R.M., 2012. Autophagy and lysosomal dysfunction as emerging mechanisms of nanomaterial toxicity. Part. Fibre Toxicol. 9, 20. https://doi.org/10.1186/1743-8977-9-20.
Smythe, E., Ayscough, K.R., 2006. Actin regulation in endocytosis. J. Cell. Sci. 119, 4589–4598. https://doi.org/10.1242/jcs.03247.
Doherty, G.J., McMahon, H.T., 2009. Mechanisms of endocytosis. Annu. Rev. Biochem. 78, 857–902. https://doi.org/10.1146/annurev.biochem.78.081307.110540.
Costa, M.M., Dios, S., Alonso-Gutierrez, J., Romero, A., Novoa, B., Figueras, A., 2009. Evidence of high individual diversity on myticin C in mussel (*Mytilus galloprovincialis*). Dev. Comp. Immunol. 33, 162–170. https://doi.org/10.1016/j.dci.2008.08.005.
Kreisel, D., Nava, R.G., Li, W., Zinselmeyer, B.H., Wang, B., Lai, J., Pless, R., Gelman, A.E., Krupnick, A.S., Miller, M.J., 2010a. In Vivo Two-photon Imaging Reveals Monocyte-dependent Neutrophil Extravasation During Pulmonary Inflammation. https://doi.org/10.1073/pnas.1008737107.
Kreisel, D., Nava, R.G., Li, W., Zinselmeyer, B.H., Wang, B., Lai, J., Pless, R., Gelman, A.E., Krupnick, A.S., Miller, M.J., 2010b. In vivo two-photon imaging reveals monocyte-dependent neutrophil extravasation during pulmonary inflammation. Proc. Natl. Acad. Sci. U. S. A. 107, 18073–18078. https://doi.org/10.1073/pnas.1008737107.
Graham, D.B., Zinselmeyer, B.H., Mascarenhas, F., Delgado, R., Miller, M.J., Swat, W., 2009. ITAM signaling by Vav family rho guanine nucleotide exchange factors regulates interstitial transit rates of neutrophils in Vivo. PLoS One 4. https://doi.org/10.1371/journal.pone.0004652.
White, E.E., Pai, A., Weng, Y., Suresh, A.K., Van Haute, D., Pailevanian, T., Alizadeh, D., Hajimiri, A., Badie, B., Berlin, J.M., 2015. Functionalized iron oxide nanoparticles for controlling the movement of immune cells. Nanoscale. 7, 7780–7789. https://doi.org/10.1039/C3NR04421A.
Gestal, C., Roch, P., Renault, T., Pallavicini, A., Paillard, C., Novoa, B., Oubella, R., Venier, P., Figueras, A., 2008. Study of diseases and the immune system of bivalves using molecular biology and genomics. Rev. Fish. Sci. Aquac. 16, 131–154. https://doi.org/10.1080/10641260802325518.
Pezzati, E., Canesi, L., Damonte, G., Salis, A., Marsano, F., Grande, C., Vezzulli, L., Pruzzo, C., 2015. Susceptibility of *Vibrio aestuarianus* 01/032 to the antibacterial activity of *Mytilus* haemolymph: identification of a serum opsonin involved in mannose-sensitive interactions. Environ. Microbiol. 17, 4271–4279. https://doi.org/10.1111/1462-2920.12750.
Benabdelmouna, A., Garcia, C., Ledu, C., Lamy, P., Maurouard, E., Dégremont, L., 2018. Mortality investigation of *Mytilus edulis* and *Mytilus galloprovincialis* in France: an experimental survey under laboratory conditions. Aquaculture. 495, 831–841. https://doi.org/10.1016/j.aquaculture.2018.06.075.
Pallavicini, A., del Mar Costa, M., Gestal, C., Dreos, R., Figueras, A., Venier, P., Novoa, B., 2008. High sequence variability of myticin transcripts in hemocytes of immune-stimulated mussels suggests ancient host–pathogen interactions. Dev. Comp. Immunol. 32, 213–226. https://doi.org/10.1016/j.dci.2007.05.008.
Balseiro, P., Falcó, A., Romero, A., Dios, S., Martínez-López, A., Figueras, A., Estepa, A., Novoa, B., 2011. *Mytilus galloprovincialis* Myticin C: a chemotactic molecule with antiviral activity and immunoregulatory properties. PLoS One 6, e23140. https://doi.org/10.1371/journal.pone.0023140.
Martinez-Lopez, A., Encinar, J.A., Medina-Gali, R.M., Balseiro, P., Garcia-Valtanen, P., Figueras, A., Novoa, B., Estepa, A., 2013. PH-dependent solution structure and activity of a reduced form of the host-defense peptide myticin C (Myt C) from the mussel *Mytilus galloprovincialis*. Mar. Drugs 11, 2328–2346. https://doi.org/10.3390/md11072328.
Novoa, B., Romero, A., Álvarez, Á.L., Moreira, R., Pereiro, P., Costa, M.M., Dios, S., Estepa, A., Parra, F., Figueras, A., 2016. Antiviral activity of myticin c peptide from mussel: an ancient defense against herpesviruses. J. Virol. 90, 7692–7702. https://doi.org/10.1128/jvi.00591-16.
Rey-Campos, M., Moreira, R., Valenzuela-Muñoz, V., Gallardo-Escárate, C., Novoa, B., Figueras, A., 2019. High individual variability in the transcriptomic response of Mediterranean mussels to *Vibrio* reveals the involvement of myticins in tissue injury. Sci. Rep. 9, 1–15. https://doi.org/10.1038/s41598-019-39870-3.